Isaindigotone Derivatives: A New Class of Highly Selective Ligands for Telomeric G-Quadruplex DNA

ARTICLE *in* JOURNAL OF MEDICINAL CHEMISTRY · MAY 2009

Impact Factor: 5.45 · DOI: 10.1021/jm801600m · Source: PubMed

10 AUTHORS, INCLUDING:

Jinqiang Hou
London Health Sciences Centre
26 PUBLICATIONS **483** CITATIONS
SEE PROFILE

Hai-Bin Luo
Sun Yat-Sen University
77 PUBLICATIONS **865** CITATIONS
SEE PROFILE

Jianyong Wu
The Hong Kong Polytechnic University
112 PUBLICATIONS **2,369** CITATIONS
SEE PROFILE

Zhishu Huang
Sun Yat-Sen University
174 PUBLICATIONS **2,282** CITATIONS
SEE PROFILE

Isaindigotone Derivatives: A New Class of Highly Selective Ligands for Telomeric G-Quadruplex DNA

Jia-Heng Tan,[†,‡] Tian-Miao Ou,[†,‡] Jin-Qiang Hou,[‡] Yu-Jing Lu,[‡] Shi-Liang Huang,[‡] Hai-Bin Luo,[‡] Jian-Yong Wu,[§] Zhi-Shu Huang,[‡,*] Kwok-Yin Wong,[§] and Lian-Quan Gu[‡,*]

School of Pharmaceutical Sciences, Sun Yat-sen University, Guangzhou 510080, China, Department of Applied Biology and Chemical Technology and the Central Laboratory of the Institute of Molecular Technology for Drug Discovery and Synthesis, The Hong Kong Polytechnic University, Hung Hom, Kowloon, Hong Kong, China

Received December 18, 2008

Four isaindigotone derivatives (**5a**,**b** and **6a**,**b**) designed as telomeric G-quadruplex ligands have been synthesized and characterized. The unfused aromatic rings in these compounds allow a flexible and adaptive conformation in G-quadruplex recognition. The interaction of human telomeric G−quadruplex DNA with these designed ligands was explored by means of FRET melting, fluorescence titration, CD spectroscopy, continuous variation, and molecular modeling studies. Our results showed that the adaptive scaffold might not only allow the ligands to well occupy the G-quartet but also perfectly bind to the grooves of the G-quadruplex. The synergetic effect of the multiple binding modes might be responsible for the improved binding ability and high selectivity of these ligands toward G-quadruplex over duplex DNA. Long-term exposure of HL60 and CA46 cancer cells to compound **5a** showed a remarkable decrease in population growth, cellular senescence phenotype, and shortening of the telomere length, which is consistent with the behavior of an effective telomeric G-quadruplex ligand and telomerase inhibitor.

1. Introduction

Human telomeric DNA, located at the very end of chromosomes, consists of tandem repeats of sequence d[(TTAGGG)$_n$], which ends as the single strand.[1] This guanine-rich single strand can adopt higher-order and functionally useful structures called the G-quadruplexes.[2,3] The building blocks of G-quadruplexes are the G-quartets (Figure 1a), which stack up with one on top of another to form such secondary DNA structures.[4]

Induction and stabilization of the telomeric G-quadruplexes by small molecules have been shown to interfere telomere biological functions, inhibit telomerase activity, and eventually alter telomere maintenance.[5−7] Telomere maintenance is crucial for the unlimited proliferative potential of cancer cells,[8,9] thus the design of drugs targeting at the telomeric G-quadruplex is a rational and promising approach for cancer chemotherapy.[10−12] However, further efforts in appropriate drug design are needed to control the G-quadruplex selectivity over duplex DNA because ligand interaction with duplex DNA leads to acute toxic and intolerable side effects on normal tissues.[13] Several small molecules, such as trisubstituted anilinoacridines and telomestatin, have been identified to selectively bind and stabilize the telomeric G-quadruplex DNA in vitro.[14,15]

Isaindigotone (Figure 1b) is a naturally occurring alkaloid. It is isolated from the root of *Isatis indigotica* Fort (Ban-Lan-Gen in Chinese), which is commonly used in traditional Chinese medicine for treatment of influenza, epidemic hepatitis, and epidemic encephalitis.[16] The structure of isaindigotone comprises a pyrrolo[2,1-*b*]quinazoline moiety conjugated with a benzylidene group. Such a compound is neither polycyclic nor macrocyclic and has free rotation around the double bond that enables the adoption of possible twisted and coplanar conformations of the aryl groups. Hence, this adaptive structural feature might allow the unfused aromatic scaffold not only to occupy the G-quartet but also bind to the grooves of G-quadruplex.[17,18] Both the G-quartet and groove regions are binding sites for a ligand selectively targeting the G-quadruplex.[13] In view of this feature, and enlightened by the tempting G-quadruplex selectivity exhibited by several unfused aromatic compounds such as 1,4-triazole derivatives,[19] biarylpyrimidines,[20] triarylpyridines,[17] and diarylethynyl amides,[18] we perceived that isaindigotone might offer an attractive template for the design of selective G-quadruplex ligands. Furthermore, isaindigotone possesses a unique asymmetric chromophore with an aliphatic five-member ring in the middle core. This scaffold would be a new type of unfused aromatic G-quadruplex ligands. The scaffold itself alone, however, is probably not sufficient as a selective and effective G-quadruplex ligand, as previous experience indicated that the presence of at least two cationic side chains to the chromophore is usually required to gain high G-quadruplex DNA binding potency and selectivity as well as the solubility in aqueous medium.[21,22]

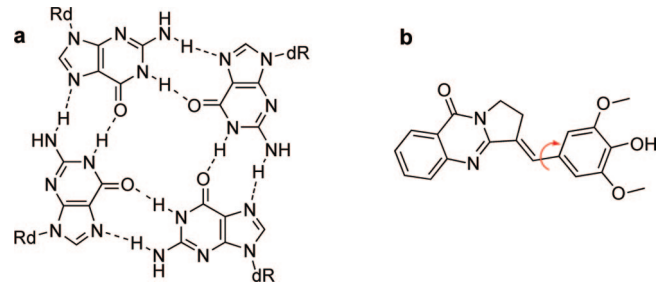

Figure 1. Structures of G-quartet (a) and isaindigotone (b).

To explore novel and selective G-quadruplex ligands for cancer chemotherapy, we have therefore synthesized a series

* To whom correspondence should be addressed. Phone: 8620-39943056 (Z.-S.H.); 8620-39943055 (L.-Q.G.). Fax: 8620-39943056 (Z.-S.H. and L.-Q.G.). E-mail: ceshzs@mail.sysu.edu.cn (Z.-S.H.); cesglq@mail.sysu.edu.cn (L.-Q.G.).

† These authors contributed equally to this paper.

‡ School of Pharmaceutical Sciences, Sun Yat-sen University.

§ Department of Applied Biology and Chemical Technology and the Central Laboratory of the Institute of Molecular Technology for Drug Discovery and Synthesis, The Hong Kong Polytechnic University.

10.1021/jm801600m CCC: $40.75
Published on Web 04/08/2009

Scheme 1. Synthesis of Isaindigotone Derivatives[a]

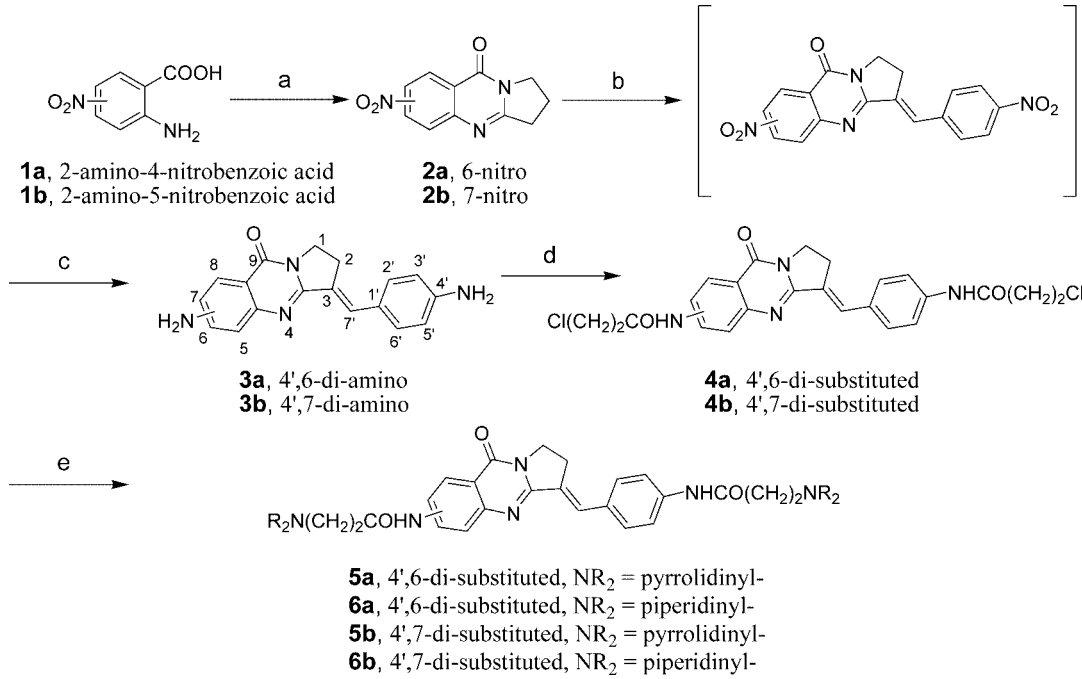

[a] Reagents: (a) pyrrolidin-2-one, $POCl_3$, toluene (reflux); (b) 4-nitrobenzaldehyde, Ac_2O (reflux); (c) $Na_2S \cdot 9H_2O$, NaOH, EtOH (reflux); (d) $Cl(CH_2)_2COCl$ (reflux); (e) R_2NH, KI, ethanol (reflux).

of new isaindigotone derivatives by attaching cationic amino side chains to the unfused aromatic chromophore. Their interactions with telomeric G-quadruplex DNA as well as the inhibitory effect on telomerase activity were examined by biophysical and biochemical assays, and the ligand−quadruplex interaction was further investigated by molecular modeling studies. In addition, cellular studies were employed to evaluate the cell senescence and telomere shortening effect induced by the new quadruplex ligands.

2. Results and Discussion

2.1. Synthesis of Isaindigotone Derivatives. The facile synthetic pathway for isaindigotone derivatives is shown in Scheme 1. Compound **2a** was prepared by the condensation of 2-amino-4-nitrobenzoic acid (**1a**) and pyrrolidin-2-one in the presence of $POCl_3$. Treatment of **2a** with 4-nitrobenzaldehyde yielded the dinitro intermediate product by Claisen−Schmidt condensation.[23] Without further purification, the product was reduced to the corresponding diamino compound **3a**. Compound **3a** was assigned as the *E* configuration on the basis of NOE[a] analysis. In the NOE experiment, upon irradiation of proton 7′-H of **3a**, only enhancement of the equivalent protons 2′-H and 6′-H was observed. Besides, upon irradiation of 2′-H and 6′-H, signals of protons 7′-H and 2-H were simultaneously enhanced (Supporting Information). Further acylation of **3a** with 3-chloropropionyl chloride gave compound **4a**. The target compounds **5a** and **6a** were then prepared by substitution of **4a** with appropriate secondary amines. Synthesis of position isomers **5b** and **6b** was accomplished following the same procedures from 2-amino-5-nitrobenzoic acid (**1b**).

[a] Abbreviations: FRET, fluorescence resonance energy transfer; CD, circular dichroism; MD, molecular dynamics; TRAP, telomere repeat amplification protocol; SA-β-Gal, senescence-associated β-galactosidase; TRF, telomeric restriction fragment; NOE, nuclear overhauser effect; EMSA, electrophoretic mobility shift assays; IC_{50}, 50% inhibitory concentration; T_m, the temperature of midtransition; rmsd, root-mean-square deviation.

Table 1. Stabilization Temperatures (ΔT_m) Determined by FRET Experiment and Equilibrium Binding Constants (K_b) by Fluorescence Titration

	ΔT_m (°C) at 1 μM ligand concentration[a]		K_b (× 10^6 M^{-1})[b]
compd	F21T	F10T	HTG21
5a	21.9 ± 1.2	0.1 ± 0.1	10.1 ± 0.6
6a	22.0 ± 0.7	0.0 ± 0.0	9.8 ± 0.4
5b	17.6 ± 1.6	0.4 ± 0.1	7.2 ± 0.8
6b	17.6 ± 0.9	0.1 ± 0.1	8.1 ± 1.0
SYUIQ-5	10.4 ± 0.2	5.7 ± 0.1	nd

[a] $\Delta T_m = T_m$ (DNA + ligand) − T_m (DNA). The concentrations of F21T and F10T were both 0.2 μM. In the absence of ligand, T_m values of annealed F21T and F10T are 60 and 64 °C, respectively. Isaindigotone was not included due to its poor solubility. [b] nd: Not determined.

The free-base form of compounds **5a**,**b** and **6a**,**b** were converted into the hydrochloride salts by treatment with hydrochloride acid in ethanol to enhance the chemical stability and aqueous solubility for the following assays.

2.2. FRET and Fluorescence Titration Studies. To evaluate the stabilization and selectivity of isaindigotone derivatives for telomeric G-quadruplex DNA, FRET melting experiments were carried out and the quindoline derivative SYUIQ-5 previously reported by us was used as a reference compound.[24−27]

Table 1 shows the effect of derivatives on the enhanced melting temperature (ΔT_m) of two labeled oligonucleotides in K^+ solution, and Figure 2A gives the concentration dependent melting curves for compounds **5a** and **5b**. F21T (5′-*FAM*-d(GGG[TTAGGG]$_3$)-*TAMRA*-3′) represents the human telomeric DNA sequence, while F10T (5′-*FAM*-dTATAGCTATA-HEG-TATAGCTATA-*TAMRA*-3′) is a hairpin duplex DNA. The FRET-melting data demonstrate that all of the derivatives effectively stabilize the telomeric G-quadruplex. At 1 μM of ligands, the ΔT_m values are in the range of 17.6−22.0 °C, which is much higher than that of the reference compound SYUIQ-5. The 4′,6-disubstituted isomers **5a** and **6a** were shown to be better quadruplex stabilizers as compared with the 4′,7-disubstituted isomers (**5b** and **6b**). On the other hand, no significant effect

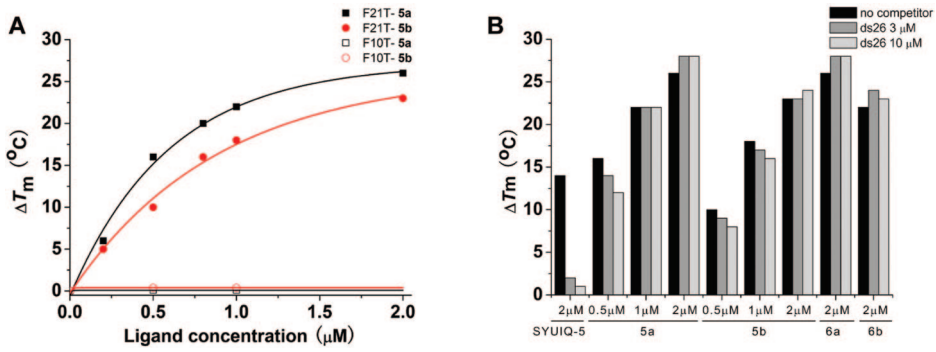

Figure 2. (A) Concentration dependent melting curves (ΔT_m vs ligand concentration) for ligands **5a** and **5b** upon binding to F21T and F10T. (B) Competitive FRET results for ligands **5a**,**b** (0.5, 1, and 2 μM), **6a**,**b**, and SYUIQ-5 (2 μM), without (black) and with 15-fold (3 μM; dark-gray) or 50-fold (10 μM; light-gray) excess of duplex DNA competitor (ds26). The concentration of F21T was 0.2 μM.

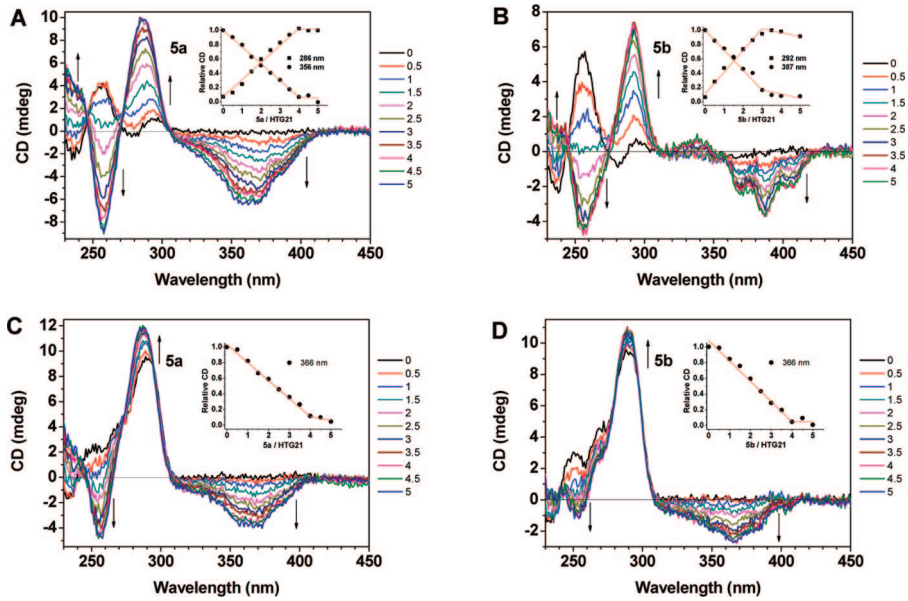

Figure 3. CD titration spectra of HTG21 (5 μM) at increasing concentrations (arrows: 0−5 mol equiv) of **5a** and **5b** in 10 mM Tris-HCl buffer, pH 7.2, without (A,B) and with (C,D) 100 mM KCl. Changes in ellipticity at characteristic wavelengths (288 and 368 nm for A and B, 366 nm for C and D) as functions of ligand/HTG21 molar ratio were plotted in the inner panels.

on T_m values was observed if a pyrrolidinyl group was placed at the terminal of side chains instead of a piperidinyl group.

As shown in Table 1, **5a**,**b** and **6a**,**b** exhibit strong preference for binding to telomeric G-quadruplex than duplex DNA. None of these compounds were observed to significantly increase the melting temperature of F10T, suggesting their poor binding to the duplex DNA.[18,19,28] Furthermore, the G-quadruplex selectivity of **5a**,**b** and **6a**,**b** was assessed by a FRET-based competition assay where the ability of ligand to retain G-quadruplex stabilizing affinity was challenged by nonfluorescent duplex DNA (ds26).[19,29] In the presence of various amounts of competitor ds26, the thermal stabilization of F21T enhanced by **5a**,**b** and **6a**,**b** was slightly affected (Figure 2A,B), while the competitor sharply disrupted the binding of SYUIQ-5 to the G-quadruplex. The combined results of these assays demonstrate that isaindigotone derivatives can be considered as a new class of highly selective G-quadruplex binding ligands.

Equilibrium binding constants (K_b) were measured by fluorescence titration assay.[30] Oligonucleotide d[$G_3(T_2AG_3)_3$] (HTG21) was used as the telomeric sequence. As shown in Table 1, all of isaindigotone derivatives exhibit high affinity for the preformed G-quadruplex DNA in K^+ solution, and in parallel with FRET results, 4′,6-disubstituted isomers **5a** and **6a** showed stronger quadruplex affinity and their binding constants are around 1.0×10^7 M^{-1}.

2.3. CD Studies. Circular dichroism (CD) spectroscopy was used to investigate the binding property of the isaindigotone derivatives to telomeric G-quadruplex.[31]

In the absence of salt, the CD spectrum of randomized HTG21 oligonucleotide was found to have a negative band centered at 238 nm, a major positive band at 257 nm, a minor negative band at 280 nm, and a positive band at near 295 nm (Figure 3A,B, black line).[32] Upon titration with **5a**, dramatic changes in the CD spectra were observed (Figure 3A). The bands at 238 and 257 nm gradually disappeared with addition of compound and eventually led to the appearance of a positive band at 240 nm and a major negative band at 258 nm, while the band centered at 292 nm significantly increased and shifted toward 286 nm. These changes are consistent with the induction of the guanine-rich DNA to form the G-quadruplex structure by compound **5a**.[32,33] Meanwhile, a strong and negative induced CD signal was observed between 310 and 410 nm. The induced CD signal was additional evidence for the interaction between the G-quadruplex and compound **5a** because its appearance in the CD spectra is indicative of an achiral ligand binding tightly to a chiral host.[34] Also, the stoichiometry of the binding of

isaindigotone derivative to G-quadruplex could be determined from CD spectra.[28,32,35,36] The changes in ellipticity at 288 and 368 nm as a function of **5a**/HTG21 were plotted on an inner panel, and the inflection point observed in each curve was indicative of the reliable formation of a 4:1 **5a**−oligonucleotide complex.

The CD spectra of compound **5b** titrated into the HTG21 oligonucleotide in the absence of salt were similar to that of **5a** in the wavelength region below 300 nm (Figure 3B). In the region of 300−450 nm, a strong and biphasic induced CD signal of **5b** with a triple negative peak centered at 387 nm and a minor positive band at near 340 nm was observed. Besides, **5b** exhibits a 3:1 stoichiometry binding to the HTG21. These results indicated that compound **5b** could also induce the guanine-rich DNA to form the G-quadruplex structure. In addition, ligand-induced formation of telomeric G-quadruplex in the absence of salt was further proved by EMSA and thermodynamic stability experiments (Supporting Information).

In the presence of K^+, HTG21 oligonucleotide forms the hybrid-type G-quadruplex structure.[37−39] The CD spectrum of such preformed structure shows a strong positive band at 290 nm, a minor positive band at 265 nm, and a negative band at 235 nm (Figure 3C,D, black line).[40] Upon titration of **5a** into this DNA solution, the CD spectra changed with enhancement of the maximum at 290 nm and suppression of the band at 265 nm. A strong negative induced CD signal also emerged between 310 and 410 nm. The negative band at 366 nm gradually increased until the ratio of **5a** to HTG21 reached 4:1 (Figure 3C). Compound **5b** induced similar CD changes and also exhibited a 4:1 stoichiometry under the same experimental conditions (Figure 3D).

Results from all CD experiments showed that the strong induced CD signal and the high stoichiometry ratio appeared to be characteristic of the interaction of isaindigotone derivatives with G-quadruplex structures. Actually, the CD signal of DNA is usually localized below 300 nm, while induced CD signal above 300 nm corresponds to the absorbance of the bound ligand. Thus, the induced CD signal can be used in the investigation of binding stoichiometry and binding mode between the ligand and G-quadruplex.[18] It is interesting to note that several quadruplex ligands (e.g., telomestatin, macrocyclic oligoamide, and SYUIQ-5) have been reported to bind to telomeric G-quadruplexes in the end-stacking mode with a 2:1 ligand-oligonucleotide stoichiometry.[28,32,36] The higher stoichiometry determined here might suggest more complicated and multiple binding modes for isaindigotone derivatives. Besides the familiar end-stacking mode, groove binding and loop binding modes of the ligands are also possible. In addition, the presence of large induced CD signal in the titration spectra has been treated as evident of groove binding mode for the ligands,[18,34] which may further support our hypothesis that isaindigotone derivative binds to the quadruplex via multiple binding modes.

2.4. Continuous Variation Studies. To further validate the meaningful binding stoichiometries obtained in CD studies, continuous variation analysis (Job plot) was performed (Figure 4).[41] The point of intersection of the two best fit lines for the Job plot for **5a** with telomeric G-quadruplex (preformed HTG21 in K^+ solution) is 0.799 and for **5b** is 0.805. Both of the results gave the same binding stoichiometry of 4 mol of ligand/mol of telomeric G-quadruplex DNA, and that is consistent with the CD studies.

2.5. Molecular Modeling Studies. To gain more details on the interactions of isaindigotone derivatives with telomeric G-quadruplexes, an approach that combined molecular docking, MD simulations, and evaluation of binding affinity was performed. The parallel propeller-type X-ray G-quadruplex structure (PDB 1KF1)[42] and a mixed hybrid-type NMR G-quadruplex structure (PDB 2HY9)[43] were used as the templates for the modeling studies because they might be the more biologically relevant forms in the presence of K^+ ion.[44]

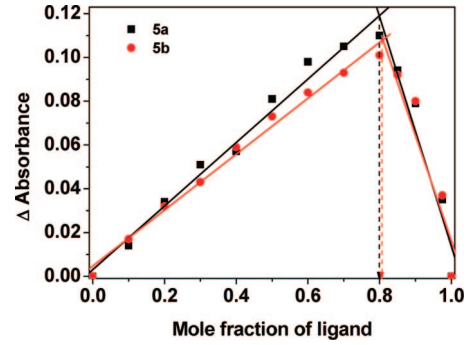

Figure 4. Job plots resulting from the method of continuous variation analysis for **5a** and **5b** with telomeric G-quadruplex DNA.

Molecular docking studies were first carried out to predict the plausible interactions between the ligands and G-quadruplex DNA. It has been previously shown that G-quadruplex binders can stack on the surface of both terminal G-quartet planes.[45] In this study, besides such end-stacking interactions, docking results also showed that such flexible ligands could be readily accommodated in the groove regions of both propeller-type and hybrid-type G-quadruplex DNA (Supporting Information).

On the basis of the docking results, MD simulations (8 ns) were performed on eight complexes formed by G-quadruplexes (propeller-type and hybrid-type) with ligands (**5a** and **5b**) in two binding modes (end-stacking and groove-binding). All of the models were quite stable during the dynamics runs (rmsd values, see Supporting Information). The complexes formed by G-quadruplex with **5a** are shown in Figure 5, and the estimated free energies of binding of **5a** and **5b** in MM-PBSA calculations for each model are shown in Table 2. It was found the ligand **5a** exhibited superior binding energies than that of **5b** in most of the models and that was in agreement with the change trend of FRET and fluorescence titration data. It was also noteworthy that both of the ligands possessed much more favorable groove binding interactions (lower binding free energy) with hybrid-type G-quadruplex than propeller-type G-quadruplex, and whatever binding of the ligand to the hybrid-type G-quadruplex showed much more comparable binding free energy.

In view of the binding free energies and the obtained CD and continuous variation analysis results in K^+ solution, hybrid-type G-quadruplex was chosen as the template for further studies of the multiple ligand−quadruplex interactions with 4:1 stoichiometry. Both models were quite stable during the dynamics runs (rmsd values, see Supporting Information). The complex of hybrid-type G-quadruplex with **5a** (1:4) was shown in Figure 5E,F. In the complex, two molecules stacked on both 5′ and 3′ G-quartet planes and the other two were deeply bound in two grooves of the G-quadruplex. The binding fashion of central pharmacophore, tertiary amine side chains, and the amide groups was similar with that in 1:1 ligand−quadruplex interactions. Meanwhile, the average binding free energies of four **5a** molecules exhibited much superior binding energies than that of **5b** (Table 2). The finding was additional evidence for the parallel correlations between FRET, fluorescence titration data, and calculated binding free energy. We recognize exact binding modes could only be identified by NMR or crystal studies.

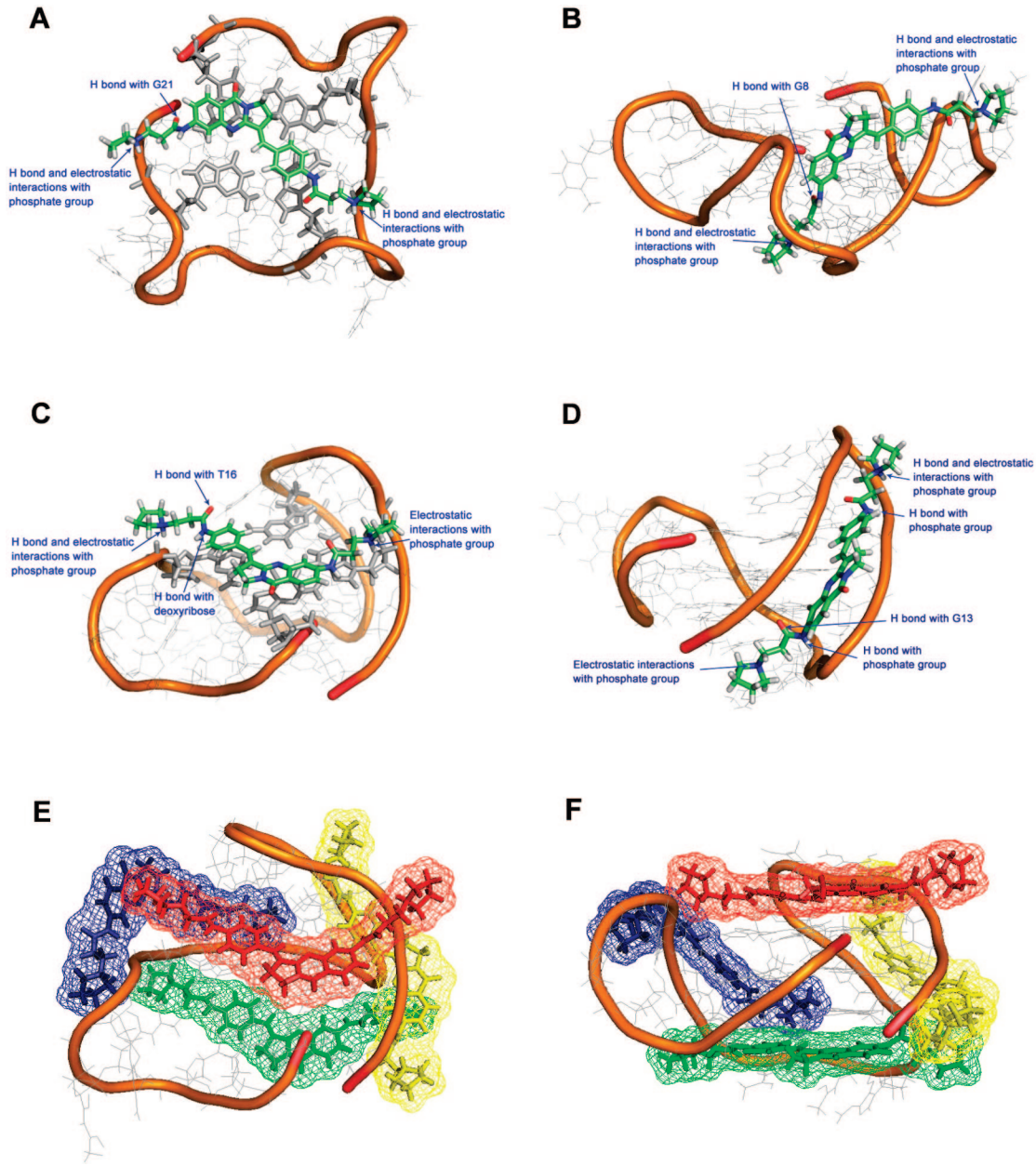

Figure 5. Models of **5a**−quadruplex complex. (A,B) **5a** stacking on the surface of G-quartet or binding to the groove of propeller-type G-quadruplex with 1:1 stoichiometry. (C,D) **5a** stacking on the surface of G-quartet or binding to the groove of hybrid-type G-quadruplex with 1:1 stoichiometry. (E,F) Top and side view of **5a** binding to the hybrid-type G-quadruplex via multiple binding modes with 4:1 stoichiometry.

Table 2. Estimated Free Energy of Binding (ΔG, in kcal·mol^{-1}) in MM-PBSA Calculations[a]

	ΔG/kcal·mol^{-1}				
	propeller-type G-quadruplex		hybrid-type G-quadruplex		
compd	end-stacking (1:1)	groove-binding (1:1)	end-stacking (1:1)	groove-binding (1:1)	multiple-binding (4:1)
5a	−42.23	−31.73	−48.41	−46.16	−43.76[a]
5b	−37.19	−32.99	−46.24	−45.60	−40.19[a]

[a] Average free binding energy per molecule.

However, these MD results in combination with the data obtained from CD and continuous variation analysis might reinforce the hypothesis that isaindigotone derivatives bound to telomeric G-quadruplex via multiple binding modes.

After an array of biophysical studies, it was necessary to clarify the molecular basis for the high selectivity of isaindigotone derivatives. Because of the geometrical freedom arising from the rotatable bond, the central pharmacophore of these ligands could adopt different conformations (i.e., coplanar and noncoplanar) for G-quadruplex recognition. The high selectivity of isaindigotone derivatives might first be attributed to their long dimension of the putatively coplanar chromophore, which matches the G-quartet better than that of the base pair of duplex DNA (Supporting Information). On the other hand, the selectivity might also be a consequence of geometrical freedom and bulkiness of the aliphatic five-member ring of these compounds, which do not allow intercalative binding into duplex DNA to take place.[19] Such reliable end-stacking of compounds onto the

Table 3. Telomerase Inhibition by Isaindigotone Derivatives in Cell-Free Assay

	5a	6a	5b	6b
$^{Tel}IC_{50}$ (μM)	7.8	9.3	9.0	15.2

G-quartet are in agreement with previous unfused aromatic quadruplex ligands.[46,47] Second, besides the end-stacking binding mode, isaindigotone derivatives might bind to the grooves of G-quadruplex DNA. Because the grooves of quadruplex DNA have different groove geometries from duplex DNA as well as different patterns of donor−acceptor sites, it has been reported that compounds bound to the quadruplex grooves should be able to achieve excellent structure-specific recognition affinity and specificity.[18,34] Thanks to the rotatable bond, the unfused aromatic chromophore in the quadruplex groove can be twisted to form the suitable noncoplanar conformation for well fitting groove geometry and maximizing H-bond intermolecular interactions. Such specific ligand−quadruplex interactions might also contribute to the high selectivity of isaindigotone derivatives. Meanwhile, different positional attachment of the side chains did not influence selectivity and the multiple binding modes of the compounds, and that was additional evidence for the key role of their scaffold. Thus, the synergetic effect of multiple binding modes arising from isaindigotone derivatives might be the major reason for enhancing their G-quadruplex selectivity over duplex DNA.

In addition, modeling studies with duplex DNA were also performed to reinforce these arguments concerning the selectivity of ligands (Supporting Information).[47] Assessments of the binding free energies of interaction models demonstrated that binding to the G-quadruplex was significantly favored relative to duplex binding. This is consistent with the proposed G-quadruplex/duplex DNA selectivity demonstrated by these ligands in biophysical studies. These results with potential quadruplex multiple-binding compounds provide a new choice for design of highly selective G-quadruplex ligands.

2.6. Telomerase Inhibition. The ability of isaindigotone derivatives to inhibit human telomerase activity were evaluated by a modified TRAP assay, the TRAP-LIG assay,[48] because the original TRAP assay was reported to suffer from interference by ligands associated with the PCR step.[49] In the experiments, solutions of derivatives were added to the telomerase reaction mixture containing extract from cracked MCF-7 breast carcinoma cell lines, and the inhibitory concentrations by half ($^{Tel}IC_{50}$) values of these compounds are listed in Table 3. It was found that all of the compounds were effective inhibitors of human telomerase ($^{Tel}IC_{50}$ values ranging from 7.8 to 15.2 μM). In parallel with above biophysical studies, compound **5a** exhibited the best inhibitory effect to the enzyme.

2.7. Senescence Induction. To examine the effects of representative compound **5a** on leukemia cell HL60 and lymphoma cell CA46, short-term cell viability was first determined in a 2-day cytotoxic assay (MTT assay). The results show that **5a** has a potent inhibitory effect, with an IC_{50} value of 33 μM in HL60 cells and 29 μM in CA46 cells.

To evaluate the long-term effects of **5a** on these cancer cells, subcytotoxic concentrations (0.9, 1.8, and 4.5 μM) of **5a** were employed to avoid acute cytotoxicity and other nonspecific events that could lead to difficulty in result interpretation. Upon treatment of HL60 cells with 4.5 μM **5a**, a significantly inhibitory effect was found after 8 days and the growth was halted after 12 days. At 1.8 μM, a delayed effect was also observed, with the number of population doublings significantly decreased after 12 days, and even with 0.9 μM **5a**, a discernible difference was observed between the control and treated cells (Figure 6A). Equally comparable results were also observed in CA46 cells (Figure 6B).

Morphologic examination of the cells during long-term cell studies displayed an increased proportion of enlarged and flattened cells with phenotypic characteristics of senescence.[50,51] These flattened cells also stained positively for the senescence-associated β-galactosidase (SA-β-Gal) activity after continuous **5a** treatment (Figure 7).[14] As a result, compound **5a** induced accelerated senescence in both cancer cell lines.

2.8. Telomere Shortening. Treatment of cancer cells with telomeric G-quadruplex ligands have been previously reported to disrupt telomere length maintenance and caused telomeres to erode.[52−54] To investigate whether representative isaindigotone derivative **5a** could cause telomeres to shorten, the telomere length was evaluated using the telomeric restriction fragment (TRF) length assay (Figure 8) on leukemia cell HL60 and lymphoma cell CA46. The results showed that 1.8 μM of **5a** triggered telomere shortening about 1.1 kb against HL60 cells, and telomere shortening was also observed after 0.9 μM of **5a** treatment. Similar reduction in telomere length was observed in CA46 cells: 1.8 μM of **5a** caused telomere shortening of about 2.3 kb against CA46 cells.

For a dysfunctional telomere that could activate p53 to initiate cellular senescence or apoptosis to suppress tumorigenesis, the induction of senescence by **5a** might result from this shortening of telomere length,[36] and this is consistent with the behavior expected for efficient telomeric G-quadruplex ligand and telomerase inhibitor.[54,55] It was reported that the cellular changes expected following exposure to telomere-targeting compounds were varied and complex, reflecting the interactions of telomeric proteins, DNA, and RNA involved in telomere maintenance. Thus, the cellular effects of **5a** could not be simply explained by telomeric G-quadruplex interactions or telomerase inhibition. Other possible telomere-independent genomic targets (promoter G-quadruplex) could be involved in drug action. Nevertheless, these compounds represented a novel group of selective G-quadruplex ligands that could be considered as useful leads for anticancer approach.

3. Conclusion

The design of drugs targeting at the telomeric G-quadruplex DNA is a rational and promising approach. On this basis, several unfused aromatic compounds have been designed, synthesized, and evaluated as effective and selective telomeric G-quadruplex ligands. The present study extended these observations to a new group of isaindigotone derivatives with an asymmetric drug-like chromophore. Our results show that isaindigotone derivatives are a promising class of telomeric G-quadruplex binding ligands with strong discrimination against the duplex DNA. Their cellular effects are also consistent with the behavior expected for efficient telomeric G-quadruplex ligand and telomerase inhibitor. Encouraged by the highly quadruplex selectivity, telomerase inhibition, and cellular effects of these ligands, more detailed investigations on the chemical biology and pharmacology of these compounds are now underway.

4. Experimental Section

Synthesis and Characterization. All chemicals were obtained from commercial sources unless otherwise specified. Melting points were determined using an X-6 microscope melting point instrument and are uncorrected. ^{1}H NMR spectra and NOESY experiment were performed on a Varian Mercury-Plus 300 NMR and INOVA 500NB spectrometry, respectively, with tetramethylsilane (TMS) as an

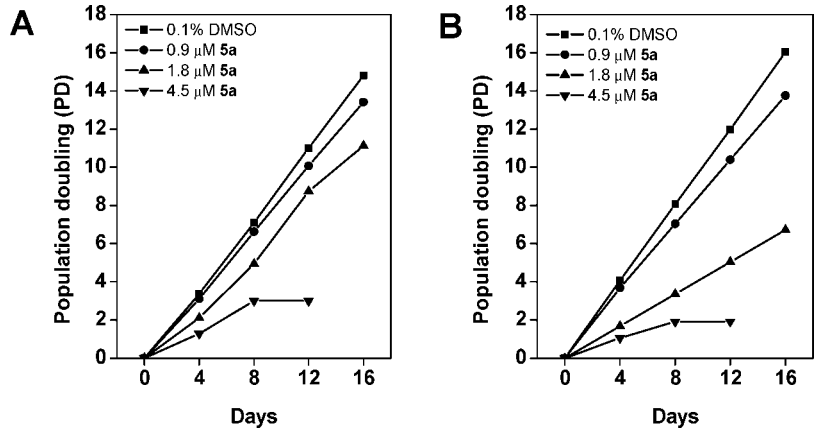

Figure 6. Long-term exposure of HL60 (A) and CA46 cells (B) with **5a** at subcytotoxic concentrations. Cells were exposed to indicated concentrations of **5a** or 0.1% DMSO, respectively. Every 4 days, the cells in control and drug-exposed flasks were counted and flasks reseeded with cells. Each experiment was performed three times at each point. This experiment was a representative of three experiments.

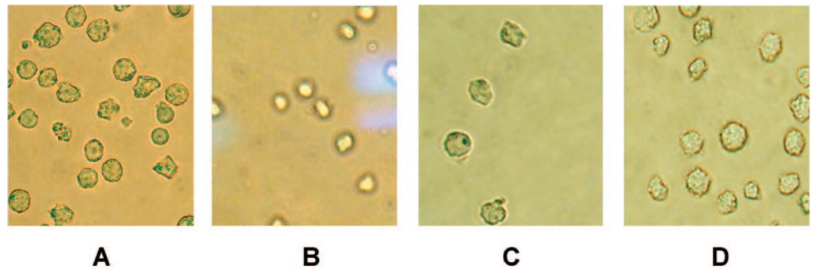

Figure 7. Expression of SA-β-Gal in HL60 and CA46 cells after continuous treatment with **5a**. HL60 cells were treated with 0.9 μM **5a** (A) or 0.1% DMSO (B) continuously for 16 days. CA46 cells were also treated with 0.9 μM **5a** (C) or 0.1% DMSO (D) continuously for 16 days. Then cells were fixed, stained with SA-β-Gal staining kit, and photographed ($\times$400). The experiment was repeated twice.

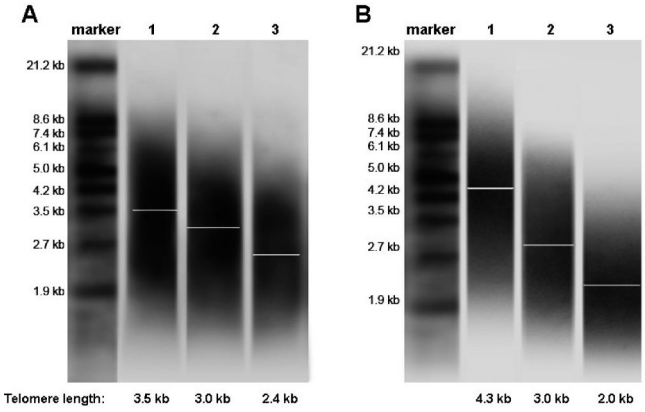

Figure 8. Effect of isaindigotone derivative **5a** on telomere length. TRF of cancer cells treated or untreated with **5a** was analyzed using the *T*elo *TAGGG* telomere length assay. (A) TRF analysis of HL60 cells treated or untreated with **5a** for 16 days. Lane 1, 0.1% DMSO; lane 2, 0.9 μM **5a**; lane 3, 1.8 μM **5a**. (B) TRF analysis of CA46 cells treated or untreated with **5a** for 16 days. Lane 1, 0.1% DMSO; lane 2, 0.9 μM **5a**; lane 3, 1.8 μM **5a**.

internal standard. ESI-MS spectra were obtained using a Thermo LCQ DECA XP LC-MS spectrometry. Elemental analysis was carried out on an Elementar Vario EL CHNS elemental analyzer, and purity of all target compounds used in the biophysical and biological studies was $\geq$95%. All compounds were routinely checked by TLC with Merck Silica Gel 60F-254 glass plates.

6-Nitro-2,3-dihydropyrrolo[2,1-*b*]quinazolin-9(1*H*)-one (2a). To a stirred suspension of pyrrolidin-2-one (0.43 g, 5 mmol) and 2-amino-4-nitrobenzoic acid (1.82 g, 10 mmol) in 250 mL anhydrous toluene, $POCl_3$ (2 mL) was added dropwise at room temperature and the mixture was refluxed for 8 h. The reaction product was poured onto ice, and then concentrated ammonium hydroxide was added to make the solution basic. The precipitate was separated from water by filtration, and the filtrate was extracted with 3 $\times$ 100 mL portions of ethyl acetate. The combined organic phase was washed with 100 mL of water containing 10 mL of concentrated ammonium hydroxide, dried over magnesium sulfate, and concentrated to dryness. The resulting residue combined with previous precipitate was purified by flash chromatography with cyclohexane/ethyl acetate (20:80) elution to afford a pale-yellow solid **2a** (0.69 g, 60%); mp 195−196 °C (lit.[56] mp 198−199 °C). ^{1}H NMR (300 MHz, $CDCl_3$) δ (ppm): 8.45 (d, J = 2.1 Hz, 1H), 8.40 (d, J = 8.7 Hz, 1H), 8.17 (dd, J = 8.7, 2.1 Hz, 1H), 4.24 (t, J = 7.2 Hz, 2H), 3.23 (t, J = 7.8 Hz, 2H), 2.30−2.40 (m, 2H). ESI-MS: m/z 232 $[M + H]^+$.

(*E*)-6-Amino-3-(4-aminobenzylidene)-2,3-dihydropyrrolo[2,1-*b*]quinazolin-9(1*H*)-one (3a). A mixture of **2a** (1.16 g, 5 mmol), 4-nitrobenzaldehyde (6.04 g, 40 mmol), and acetic anhydride (50 mL) was heated at reflux temperature for 28 h. After cooling, the precipitate was separated from solvent by filtration and rinsed with chloroform (100 mL) and acetone (200 mL) to afford a dinitro intermediate. To a stirred suspension of dinitro intermediate (1.64 g) in ethanol (50 mL) was added a solution of $Na_2S \cdot 9H_2O$ (4.8 g, 20 mmol) and NaOH (2 g, 50 mmol) in water (80 mL). The mixture was heated at reflux for 6 h and left to stand overnight. The ethanol was removed in vacuo and the residue cooled to 0−5 °C. The resulting precipitate was collected by filtration, repeatedly washed with water, and dried. Recrystallization from ethanol/acetone afforded the product **3a** (0.91 g, 60%) as an orange−red solid; mp >280 °C. ^{1}H NMR (500 MHz, DMSO-d_6) δ (ppm): 7.75 (d, J = 8.5 Hz, 1H), 7.48 (br s, 1H), 7.34 (d, J = 8.5 Hz, 2H), 6.62−6.66 (m, 4H), 5.95 (br s, 2H), 5.64 (br s, 2H), 4.05 (t, J = 7.5 Hz, 2H), 3.11−3.14 (m, 2H). ESI-MS: m/z 305 $[M + H]^+$.

(*E*)-3-Chloro-*N*-(4-((6-(3-chloropropanamido)-9-*oxo*-1,2-dihydropyrrolo[2,1-*b*]quinazolin-3(9*H*)-ylidene)methyl)phenyl)propanamide (4a). A suspension of **3a** (1.52 g, 5 mmol) in 3-chloropropanoyl chloride (10 mL) was heated at reflux for 4 h, until

TLC indicated completion of reaction. After cooling to 0−5 °C, the mixture was filtered and the crude solid washed with three 15 mL portions of ether. Recrystallization from DMF-EtOH (4:1 v/v) afforded **4a** (1.82 g, 75%) as a yellow solid; mp >280 °C. ^{1}H NMR (300 MHz, DMSO-d_6) δ (ppm): 10.55 (br s, 1H), 10.34 (br s, 1H), 8.14 (d, J = 2.1 Hz, 1H), 8.05 (d, J = 8.7 Hz, 1H), 7.73 (d, J = 8.7 Hz, 2H), 7.70 (br s, 1H), 7.63 (d, J = 8.7 Hz, 2H), 7.53 (dd, J = 8.7, 2.1 Hz, 1H), 4.16 (t, J = 6.6 Hz, 2H), 3.87−3.94 (m, 4H), 3.23−3.27 (m, 2H), 2.84−2.93 (m, 4H). ESI-MS: *m/z* 485 $[M - H]^-$.

(*E*)-*N*-(9-*oxo*-3-(4-(3-(Pyrrolidin-1-yl)propanamido)benzylidene)-1,2,3,9-tetrahydropyrrolo[2,1-*b*]quinazolin-6-yl)-3-(pyrrolidin-1-yl)propanamide (5a). To a stirred refluxing suspension of **4a** (0.25 g, 0.5 mmol) and KI (0.05 g) in EtOH (10 mL) was added dropwise pyrrolidine (0.35 mL, 5 mmol) in EtOH (1.6 mL). The mixture was stirred at reflux for 3 h, cooled to 0 °C, filtered, and washed with ether (10 mL). Recrystallization from $CHCl_3$-EtOH (2:1 v/v) gave **5a** (0.19 g, 70%) as a pale-yellow solid; mp 183−185 °C. ^{1}H NMR (300 MHz, $CDCl_3$) δ (ppm): 11.64 (br s, 1H), 11.45 (br s, 1H), 8.22 (d, J = 8.7 Hz, 1H), 7.80 (t, J = 2.4 Hz, 1H), 7.78 (d, J = 2.1 Hz, 1H), 7.68 (dd, J = 8.7, 2.1 Hz, 1H), 7.59 (d, J = 8.7 Hz, 2H), 7.52 (d, J = 8.7 Hz, 2H), 4.29 (t, J = 6.9 Hz, 2H), 3.27−3.32 (m, 2H), 2.90−2.94 (m, 4H), 2.64−2.80 (m, 8H), 2.59−2.64 (m, 4H), 1.95−1.98 (m, 8H). ESI-MS: *m/z* 555 $[M + H]^+$. Trihydrochloride salt, anal. ($C_{32}H_{38}N_6O_3 \cdot 3HCl \cdot 3.5H_2O$) C, H, N.

(*E*)-*N*-(9-*oxo*-3-(4-(3-(Piperidin-1-yl)propanamido)benzylidene)-1,2,3,9-tetrahydropyrrolo[2,1-*b*]quinazolin-6-yl)-3-(piperidin-1-yl)propanamide (6a). Following the method for production of **5a**, a yellow solid **6a** (0.20 g, 68%) was obtained; mp 179−182 °C. ^{1}H NMR (300 MHz, $CDCl_3$) δ (ppm): 11.70 (br s, 1H), 11.58 (br s, 1H), 8.20 (d, J = 8.7 Hz, 1H), 7.86 (d, J = 1.8 Hz, 1H), 7.79 (br s, 1H), 7.64 (dd, J = 8.7, 1.8 Hz, 1H), 7.62 (d, J = 8.7 Hz, 2H), 7.51 (d, J = 8.4 Hz, 2H), 4.26 (t, J = 7.2 Hz, 2H), 3.25−3.30 (m, 2H), 2.67−2.71 (m, 4H), 2.52−2.58 (m, 12H), 1.71−1.76 (m, 8H), 1.50−1.63 (m, 4H). ESI-MS: *m/z* 583 $[M + H]^+$. Trihydrochloride salt, anal. ($C_{34}H_{42}N_6O_3 \cdot 3HCl \cdot 5H_2O$) C, H, N.

Using the 2-amino-5-nitrobenzoic acid as the starting material and following the method for production of **2a**−**6a**, compounds **2b**−**6b** were synthesized.

7-Nitro-2,3-dihydropyrrolo[2,1-*b*]quinazolin-9(1*H*)-one (2b). A pale-yellow solid **2b** (0.75 g, 65%); mp 191−192 °C (lit.[57] mp 187−188 °C). ^{1}H NMR (300 MHz, $CDCl_3$) δ (ppm): 9.11 (d, J = 2.7 Hz, 1H), 8.48 (dd, J = 8.7, 2.7 Hz, 1H), 7.72 (d, J = 8.7 Hz, 1H), 4.24 (t, J = 7.2 Hz, 2H), 3.23 (t, J = 7.8 Hz, 2H), 2.29−2.40 (m, 2H). ESI-MS: *m/z* 232 $[M + H]^+$.

(*E*)-7-Amino-3-(4-aminobenzylidene)-2,3-dihydropyrrolo[2,1-*b*]quinazolin-9(1*H*)-one (3b). An orange−red solid **3b** (0.94 g, 62%); mp >280 °C. ^{1}H NMR (500 MHz, DMSO-d_6) δ (ppm): 7.42 (br s, 1H), 7.40 (d, J = 8.5 Hz, 1H), 7.31 (d, J = 8.5 Hz, 2H), 7.22 (d, J = 2.5 Hz, 1H), 7.07 (dd, J = 8.5, 2.5 Hz, 1H), 6.64 (d, J = 8.5 Hz, 2H), 5.56 (br s, 4H), 4.11 (t, J = 7.5 Hz, 2H), 3.13−3.16 (m, 2H). ESI-MS: *m/z* 305 $[M + H]^+$.

(*E*)-3-Chloro-*N*-(4-((7-(3-chloropropanamido)-9-*oxo*-1,2-dihydropyrrolo[2,1-*b*]quinazolin-3(9*H*)-ylidene)methyl)phenyl)propanamide (4b). A yellow solid **4b** (1.60 g, 66%); mp >280 °C. ^{1}H NMR (300 MHz, DMSO-d_6) δ (ppm): 10.49 (br s, 1H), 10.36 (br s, 1H), 8.50 (d, J = 2.4 Hz, 1H), 7.96 (dd, J = 8.7, 2.4 Hz 1H), 7.72−7.76 (m, 4H), 7.61 (d, J = 9 Hz, 2H), 4.20 (t, J = 7.1 Hz, 2H), 3.87−3.93 (m, 4H), 3.24−3.29 (m, 2H), 2.84−2.90 (m, 4H). ESI-MS: *m/z* 519 $[M + Cl]^-$.

(*E*)-*N*-(9-*oxo*-3-(4-(3-(pyrrolidin-1-yl)propanamido)benzylidene)-1,2,3,9-tetrahydropyrrolo[2,1-*b*]quinazolin-7-yl)-3-(pyrrolidin-1-yl)propanamide (5b). A yellow solid **5b** (0.18 g, 66%); mp 247−248 °C. ^{1}H NMR (300 MHz, $CDCl_3$) δ (ppm): 11.53 (br s, 1H), 11.49 (br s, 1H), 8.20 (dd, J = 9, 2.4 Hz, 1H), 8.02 (d, J = 2.4 Hz, 1H), 7.74 (t, J = 2.7 Hz, 1H), 7.68 (d, J = 9 Hz 1H), 7.55 (d, J = 9 Hz, 2H), 7.49 (d, J = 9 Hz, 2H), 4.27 (t, J = 6.9 Hz, 2H), 3.24−3.30 (m, 2H), 2.84−2.89 (m, 4H), 2.65−2.75 (m, 8H), 2.53−2.59 (m, 4H), 1.91−1.92 (m, 8H). ESI-MS: *m/z* 555 $[M + H]^+$. Trihydrochloride salt, anal. ($C_{32}H_{38}N_6O_3 \cdot 3HCl \cdot 1.5H_2O$) C, H, N.

(*E*)-*N*-(9-*oxo*-3-(4-(3-(Piperidin-1-yl)propanamido)benzylidene)-1,2,3,9-tetrahydropyrrolo[2,1-*b*]quinazolin-7-yl)-3-(piperidin-1-yl)propanamide (6b). A yellow solid **6b** (0.19 g, 65%); mp 240−241 °C. ^{1}H NMR (300 MHz, $CDCl_3$) δ (ppm): 11.69 (br s, 1H), 11.59 (br s, 1H), 8.26 (dd, J = 9, 2.4 Hz, 1H), 8.13 (d, J = 2.4 Hz, 1H), 7.77 (br s, 1H), 7.72 (d, J = 9 Hz 1H), 7.64 (d, J = 8.7 Hz, 2H), 7.53 (d, J = 8.7 Hz, 2H), 4.30 (t, J = 7.2 Hz, 2H), 3.28−3.33 (m, 2H), 2.69−2.74 (m, 4H), 2.54−2.60 (m, 12H), 1.74−1.79 (m, 8H), 1.60−1.61 (m, 4H). ESI-MS: *m/z* 583 $[M + H]^+$. Trihydrochloride salt, anal. ($C_{34}H_{42}N_6O_3 \cdot 3HCl \cdot 4H_2O$) C, H, N.

Materials. All oligomers/primers used in this study were purchased from Invitrogen (China). Acrylamide/bisacrylamide solution and *N*,*N*,*N*′,*N*′-tetramethyl-ethylenediamine were purchased from Sigma. *Taq* DNA polymerase was purchased from Sangon (China). Stock solutions of all the isaindigotone derivatives (2 mM) were made using double-distilled deionized water containing 50% DMSO and stored at −80 °C. Further dilutions to working concentrations were made with relevant buffer immediately prior to use. All tumor cell lines were obtained from the American Type Culture Collection (ATCC, Rockville, MD). The cell culture was maintained in a RPMI-1640 medium supplemented with 10% fetal bovine serum, 100 U/mL penicillin, and 100 μg/mL streptomycin in 25 cm^2 culture flasks at 37 °C humidified atmosphere with 5% CO_2.

FRET Assay. FRET assay was performed as a high-throughput screen following previously published procedures.[29,36] The labeled oligonucleotides F21T:5′-*FAM*-d(GGG[TTAGGG]$_3$)-*TAMRA*-3′ and F10T:5′-*FAM*-dTATAGCTATA-HEG-TATAGCTATA-*TAMRA*-3′ (donor fluorophore *FAM* is 6-carboxyfluorescein; acceptor fluorophore *TAMRA* is 6-carboxytetramethylrhodamine; HEG linker is [(−CH_2−CH_2−O−)$_6$]) were used as the FRET probes. Fluorescence melting curves were determined with a Roche LightCycler 2 real-time PCR machine, using a total reaction volume of 20 μL, with 0.2 μM of labeled oligonucleotide in Tris-HCl buffer (10 mM, pH 7.2) containing 60 mM KCl. Fluorescence readings with excitation at 470 nm and detection at 530 nm were taken at intervals of 1 °C over the range 37−99 °C, with a constant temperature being maintained for 30 s prior to each reading to ensure a stable value. The melting of the G-quadruplex was monitored alone or in the presence of various concentrations of compounds and/or of double-stranded competitor ds26 (5′-CAATCGGATCGAATTCGATC-CGATTG-3′). Final analysis of the data was carried out using Origin 7.5 (OriginLab Corp.).

CD Measurements. CD experiments were performed on a Chirascan circular dichroism spectrophotometer (Applied Photophysics). A quartz cuvette with 4 mm path length was used for the spectra recorded over a wavelength range of 230−450 at 1 nm bandwidth, 1 nm step size, and 0.5 s time per point. The oligomer HTG21 (5′-d(GGG[TTAGGG]$_3$)-3′) was diluted from stock to the correct concentration (5 μM) in Tris-HCl buffer (10 mM, pH 7.2) with or without 100 mM KCl and then annealed by heating to 90 °C for 5 min, gradually cooled to room temperature, and incubated at 4 °C overnight. Then, CD titration was performed at a fixed HTG21 concentration (5 μM) with various concentrations (0−5 mol equiv) of the ligands in buffer with or without 100 mM KCl at 25 °C. After each addition of ligand, the reaction was stirred and allowed to equilibrate for at least 13 min (until no elliptic changes were observed) and a CD spectrum was collected. A buffer baseline was collected in the same cuvette and subtracted from the sample spectra. Final analysis of the data was carried out using Origin 7.5 (OriginLab Corp.).

Fluorescence Titration. Fluorescence titrations were performed on a Perkin-Elmer LS-55 luminescence spectrophotometer following previously published procedures at 25 °C.[58] A quartz cuvette with 1 cm × 1 cm path length was used for the spectra recorded at 5 nm excitation and emission slit widths. Small aliquots of a stock solution of HTG21 (preformed G-quadruplex) were added into the solution containing ligand at fixed concentration (2 μM) in Tris-

HCl buffer (10 mM, pH 7.2) with 100 mM KCl. The final concentration of DNA was varied from 0 to 2 μM. After each addition of DNA, the reaction was stirred and allowed to equilibrate for at least 10 min and fluorescence measurement was taken at Ex 343 nm for **5a** and **6a** or 353 nm for **5b** and **6b**. Fluorescence emission (448 nm for **5a** and **6a** or 450 nm for **5b** and **6b**) data points at each step were then obtained, and the equilibrium binding constants were derived from the Scatchard analysis.

Continuous Variation Analysis. Continuous variation analysis was performed on a Shimadzu UV-2450 spectrophotometer following previously published procedures.[41] Stock solutions of 10 μM ligand and 10 μM HTG21 were prepared in Tris-HCl buffer (10 mM, pH 7.2) containing 100 mM KCl. Two series of solutions were used for the experiments: one with varying mole fractions of ligand and HTG21, and another one with varying concentrations of ligand. The sum of the ligand and HTG21 concentrations was always 10 μM. Their absorbance spectra were collected from 300 to 500 nm using a 1 cm path length quartz cuvette at 25 °C. Absorbance of ligand solution without oligonucleotide minus that of corresponding ligand solution with oligonucleotide gave the difference spectra. Such difference in the absorbance values at λ_{max} wavelength (343 nm for **5a** and 353 nm for **5b**) was plotted versus the ligand mole fraction to generate a Job plot. Final analysis of the data was carried out using Origin 7.5 (OriginLab Corp.).

Molecular Modeling. The crystal structure of the parallel propeller-type 22-mer telomeric G-quadruplex (PDB 1KF1)[42] and the NMR structure of the mixed hybrid-type 26-mer telomeric G-quadruplex (PDB 2HY9)[43] were used as the initial templates to study the interaction between the isaindigotone derivatives and telomeric DNA. For comparison with the d(GGG[TTAGGG]$_3$) DNA we used in the FRET and CD experiments, we removed the terminal 5′ adenine residue from the propeller-type structure and five adenines from each end of the hybrid-type structure to generate the 21-mer structures. Water molecules were removed from the PDB file, whereas the missing hydrogen atoms were added to the system using the Biopolymer module implemented in the SYBYL7.3.5 molecular modeling software from Tripos Inc. (St. Louis, MO). Ligand structures were constructed and optimized with GAUSSIAN 03[59] using the HF/6-31G* basis set.

Docking studies were performed using the AUTODOCK 4.0 program.[60] Using ADT,[61] nonpolar hydrogens of telomeric G-quadruplex were merged to their corresponding carbons and partial atomic charges were assigned. The nonpolar hydrogens of the ligands were merged, and rotatable bonds were assigned. The propeller-type or hybrid-type G-quadruplex structure was used as an input for the AUTOGRID program. AUTOGRID performed a precalculated atomic affinity grid maps for each atom type in the ligand plus an electrostatics map and a separate desolvation map present in the substrate molecule. The dimensions of the active site box that was placed at the center of the G-quadruplex were set to 110 Å × 110 Å × 110 Å with a grid spacing of 0.375 Å. Docking calculations were carried out using the Lamarckian genetic algorithm (LGA). Initially, we used a population of random individuals (population size: 150), a maximum number of 2500000 energy evaluations, a maximum number of generations of 27000, and a mutation rate of 0.02. Two hundred independent docking runs were done for each ligand. The resulting positions were clustered according to a root-mean-square criterion of 0.5 Å.

Molecular dynamics simulations were performed using the sander module of the AMBER 10.0 program suite. The nucleic acids studied were as treated using the parm[99] parameters.[62] Partial-atomic charges for the ligand molecules were derived using the HF/6-31G* basis set followed by RESP calculation, while force-field parameters were taken from the generalized Amber force field (GAFF)[63] using ANTECHAMBER module. The K^+ radius was kept at 2.025 Å.[64,65] Periodic boundary conditions were applied with the particle-mesh Ewald (PME) method[66] used to treat long-range electrostatic interactions. The quadruplex and ligand complexes were solvated in a rectangular box of TIP3P[67] water molecules with solvent layers 10 Å. And the potassium counterions were added to neutralize the complexes.

The hydrogen bonds were constrained using SHAKE.[68] For the nonbonded interactions, a residue-based cutoff of 10 Å was used. Temperature regulation was achieved by Langevin coupling with a collision frequency of 1.0. The solvated structures were subjected to initial minimization to equilibrate the solvent and counter cations. The G-quadruplex and inner K^+ ions were initially fixed with force constants of 100 kcal·mol^{-1}. The system was then heated from 0 to 300 K in a 100 ps simulation and followed by a 100 ps simulation to the equilibrate the density of the system. Afterward, constant pressure MD simulation of 8 ns was then performed in an NPT ensemble at 1 atm and 300 K. The output and trajectory files were saved every 0.1 and 1 ps for the subsequent analysis, respectively. All trajectory analysis was done with the Ptraj module in the Amber 10.0 suite and examined visually using the VMD software package.[69]

The MM/PBSA method[70] implemented in the AMBER 10 suite was used to calculate the binding free energy between the G-quadruplex and the isaindigotone derivatives. All the waters and counterions were stripped off but included the K^+ present within the negative charged central channel. The set of 1000 snapshots from MD trajectories were collected to calculate the binding free energies.

Molecular modeling studies of the interactions between isaindigotone derivatives with duplex DNA were performed following analogous procedures and parameters shown above. A self-complementary duplex DNA was built in SYBYL from the sequence d[(TA)$_2$GC(TA)$_2$] for these studies.[47]

TRAP-LIG Assay. The ability of isaindigotone derivatives to inhibit telomerase in a cell-free system was assessed with the TRAP-LIG assay following previously published procedures.[48] Protein extracts from exponentially growing MCF-7 breast carcinoma cells were used. Briefly, 0.1 μg of TS forward primer (5′-AATCCGTC-GAGCAGAGTT-3′) was elongated by telomerase (500 ng protein extract) in TRAP buffer (20 mM Tris-HCl [pH 8.3], 68 mM KCl, 1.5 mM $MgCl_2$, 1 mM EGTA, and 0.05% Tween 20) containing 125 μM dNTPs and 0.05 μg BSA. The mix was added to tubes containing freshly prepared ligand at various concentrations and to a negative control containing no ligand. The initial elongation step was carried out for 20 min at 30 °C, followed by 94 °C for 5 min and a final maintenance of the mixture at 20 °C. To purify the elongated product and to remove the bound ligands, the QIA quick nucleotide purification kit (Qiagen) was used according to the manufacturer's instructions. The purified extended samples were then subject to PCR amplification. For this, a second PCR master mix was prepared consisting of 1 μM ACX reverse primer (5′-GCGCGG[CTTACC]$_3$CTAACC-3′), 0.1 μg TS forward primer (5′-AATCCGTCGAGCAGAGTT-3′), TRAP buffer, 5 μg BSA, 0.5 mM dNTPs, and 2 units of *Taq* polymerase. A 10 μL aliquot of the master mix was added to the purified telomerase extended samples and amplified for 35 cycles of 94 °C for 30 s, of 61 °C for 1 min, and of 72 °C for 1 min. Samples were separated on a 16% PAGE and visualized with silver-stained. $^{Tel}IC_{50}$ values were then calculated from the optical density quantitated from the AlphaEaseFC software.

Short-Term Cell Viability. HL60 leukemia cell line and CA46 lymphoma cell line were seeded on 96-well plates (1.0×10^3/well) and exposed to various concentrations of ligand. After 48 h of treatment at 37 °C in a humidified atmosphere of 5% CO_2, 10 μL of 5 mg/mL methyl thiazolyl tetrazolium (MTT) solution was added to each well and further incubated for 4 h. The cells in each well were then treated with dimethyl sulfoxide (DMSO) (200 μL for each well), and the optical density (OD) was recorded at 570 nm. All drug doses were parallel tested in triplicate, and the IC_{50} values were derived from the mean OD values of the triplicate tests versus drug concentration curves.

Long-Term Cell Culture Experiments. Long-term proliferation experiments were carried out using the HL60 leukemia cell line and CA46 lymphoma cell line. Cells were grown in T80 tissue culture flasks at 1.0×10^5 per flask and exposed to a subcytotoxic concentration of ligand or an equivalent volume of 0.1% DMSO every 4 days. The cells in control and drug-exposed flasks were

counted and flasks reseeded with 1.0×10^5 cells. The remaining cells were collected and used for measurements described below. This process was continued for 16 days or stopped until the cell number was not enough to reseed.

SA-β-Gal Assay. Cells treated with the ligand were incubated for 16 days. After the incubation, the growth medium was aspirated and the cells were fixed in 2% formaldehyde/0.2% glutaraldehyde for 15 min at room temperature. The fixing solution was removed, and the cells were gently washed twice with PBS and then stained using the β-Gal stain solution containing 1 mg/mL of 5-bromo-4-chloro-3-indolyl-β-D-galactoside, followed by incubation overnight at 37 °C. The staining solution was removed, and the cells were washed three times with PBS. The cells were viewed under an optical microscope and photographed.

Telomere Length Assay. Cells treated with the ligand were incubated for 16 days. To measure the telomere length, genomic DNA was digested with Hinf1/Rsa1 restriction enzymes. The digested DNA fragments were separated on 0.8% agarose gel, transferred to a nylon membrane, and the transferred DNA fixed on the wet blotting membrane by baking the membrane at 120 °C for 20 min. Membrane was hybridized with a DIG-labeled hybridization probe for telomeric repeats and incubated with anti-DIG-alkaline phosphatase. TRF was performed by chemiluminescence detection.

Acknowledgment. We thank the National Nature Science Foundation of China (20772159, 90813011, U0832005), the NSFC/RGC joint Research Scheme (30731160006 and N_PolyU 508/06), the Science Foundation of Guangzhou (2006Z2-E402), the NCET, the Shenzhen Key Laboratory Fund, and the University Grants Committee Areas of Excellence Scheme in Hong Kong (AoE P/10-01) for financial support of this study.

Supporting Information Available: NOE analysis of **3a** and **3b**, elemental analysis used to determine the degree of purity for compounds, UV analysis, FRET-melting studies, fluorescence titration assay, EMSA and thermodynamic stability experiments, molecular modeling studies, and telomerase inhibition results. This material is available free of charge via the Internet at http://pubs.acs.org.

References

(1) Blackburn, E. H. Structure and function of telomeres. *Nature (London)* **1991**, *350*, 569–573.
(2) Burge, S.; Parkinson, G. N.; Hazel, P.; Todd, A. K.; Neidle, S. Quadruplex DNA: sequence, topology and structure. *Nucleic Acids Res.* **2006**, *34*, 5402–5415.
(3) Dai, J.; Carver, M.; Yang, D. Polymorphism of human telomeric quadruplex structures. *Biochimie* **2008**, *90*, 1172–1183.
(4) Davis, J. T. G-quartets 40 years later: From 5′-GMP to molecular biology and supramolecular chemistry. *Angew. Chem., Int. Ed.* **2004**, *43*, 668–698.
(5) Gomez, D.; Paterski, R.; Lemarteleur, T.; Shin-ya, K.; Mergny, J.-L.; Riou, J.-F. Interaction of telomestatin with the telomeric single-strand overhang. *J. Biol. Chem.* **2004**, *279*, 41487–41494.
(6) Burger, A. M.; Dai, F.; Schultes, C. M.; Reszka, A. P.; Moore, M. J.; Double, J. A.; Neidle, S. The G-quadruplex-interactive molecule BRACO-19 inhibits tumor growth, consistent with telomere targeting and interference with telomerase function. *Cancer Res.* **2005**, *65*, 1489–1496.
(7) De Cian, A.; Lacroix, L.; Douarre, C.; Temime-Smaali, N.; Trentesaux, C.; Riou, J.-F.; Mergny, J.-L. Targeting telomeres and telomerase. *Biochimie* **2008**, *90*, 131–155.
(8) Bryan, T. M.; Cech, T. R. Telomerase and the maintenance of chromosome ends. *Curr. Opin. Cell Biol.* **1999**, *11*, 318–324.
(9) Masutomi, K.; Yu, E. Y.; Khurts, S.; Ben-Porath, I.; Currier, J. L.; Metz, G. B.; Brooks, M. W.; Kaneko, S.; Murakami, S.; DeCaprio, J. A.; Weinberg, R. A.; Stewart, S. A.; Hahn, W. C. Telomerase maintains telomere structure in normal human cells. *Cell* **2003**, *114*, 241–253.
(10) Hurley, L. H. DNA and its associated processes as targets for cancer therapy. *Nat. Rev. Cancer* **2002**, *2*, 188–200.
(11) Neidle, S.; Parkinson, G. Telomere maintenance as a target for anticancer drug discovery. *Nat. Rev. Drug Discovery* **2002**, *1*, 383–393.
(12) Ou, T.-M.; Lu, Y.-J.; Tan, J.-H.; Huang, Z.-S.; Wong, K.-Y.; Gu, L.-Q. G-quadruplexes: targets in anticancer drug design. *ChemMedChem* **2008**, *3*, 690–713.
(13) Tan, J.-H.; Gu, L.-Q.; Wu, J.-Y. Design of selective G-quadruplex ligands as potential anticancer agents. *Mini-Rev. Med. Chem.* **2008**, *8*, 1163–1178.
(14) Moore, M. J. B.; Schultes, C. M.; Cuesta, J.; Cuenca, F.; Gunaratnam, M.; Tanious, F. A.; Wilson, W. D.; Neidle, S. Trisubstituted acridines as G-quadruplex telomere targeting agents. Effects of extensions of the 3,6- and 9-side chains on quadruplex binding, telomerase activity, and cell proliferation. *J. Med. Chem.* **2006**, *49*, 582–599.
(15) Kim, M.-Y.; Vankayalapati, H.; Shin-ya, K.; Wierzba, K.; Hurley, L. H. Telomestatin, a potent telomerase inhibitor that interacts quite specifically with the human telomeric intramolecular G-quadruplex. *J. Am. Chem. Soc.* **2002**, *124*, 2098–2099.
(16) Wu, X.; Qin, G.; Cheung, K. K.; Cheng, K. F. New alkaloids from *Isatis indigotica*. *Tetrahedron* **1997**, *53*, 13323–13328.
(17) Waller, Z. A. E.; Shirude, P. S.; Rodriguez, R.; Balasubramanian, S. Triarylpyridines: a versatile small molecule scaffold for G-quadruplex recognition. *Chem. Commun.* **2008**, 1467–1469.
(18) Dash, J.; Shirude, P. S.; Hsu, S.-T. D.; Balasubramanian, S. Diarylethynyl amides that recognize the parallel conformation of genomic promoter DNA G-quadruplexes. *J. Am. Chem. Soc.* **2008**, *130*, 15950–15956.
(19) Moorhouse, A. D.; Santos, A. M.; Gunaratnam, M.; Moore, M.; Neidle, S.; Moses, J. E. Stabilization of G-quadruplex DNA by highly selective ligands via click chemistry. *J. Am. Chem. Soc.* **2006**, *128*, 15972–15973.
(20) Wheelhouse, R. T.; Jennings, S. A.; Phillips, V. A.; Pletsas, D.; Murphy, P. M.; Garbett, N. C.; Chaires, J. B.; Jenkins, T. C. Design, synthesis, and evaluation of novel biarylpyrimidines: a new class of ligand for unusual nucleic acid structures. *J. Med. Chem.* **2006**, *49*, 5187–5198.
(21) Harrison, R. J.; Cuesta, J.; Chessari, G.; Read, M. A.; Basra, S. K.; Reszka, A. P.; Morrell, J.; Gowan, S. M.; Incles, C. M.; Tanious, F. A.; Wilson, W. D.; Kelland, L. R.; Neidle, S. Trisubstituted acridine derivatives as potent and selective telomerase inhibitors. *J. Med. Chem.* **2003**, *46*, 4463–4476.
(22) Monchaud, D.; Teulade-Fichou, M.-P. A hitchhiker's guide to G-quadruplex ligands. *Org. Biomol. Chem.* **2008**, *6*, 627–636.
(23) Molina, P.; Tarraga, A.; Gonzalez-Tejero, A.; Rioja, I.; Ubeda, A.; Terencio, M. C.; Alcaraz, M. J. Inhibition of leukocyte functions by the alkaloid isaindigotone from *Isatis indigotica* and some new synthetic derivatives. *J. Nat. Prod.* **2001**, *64*, 1297–1300.
(24) Mergny, J.-L.; Lacroix, L.; Teulade-Fichou, M.-P.; Hounsou, C.; Guittat, L.; Hoarau, M.; Arimondo, P. B.; Vigneron, J.-P.; Lehn, J.-M.; Riou, J.-F.; Garestier, T.; Helene, C. Telomerase inhibitors based on quadruplex ligands selected by a fluorescence assay. *Proc. Natl. Acad. Sci. U.S.A.* **2001**, *98*, 3062–3067.
(25) De Cian, A.; Guittat, L.; Kaiser, M.; Sacca, B.; Amrane, S.; Bourdoncle, A.; Alberti, P.; Teulade-Fichou, M.-P.; Lacroix, L.; Mergny, J.-L. Fluorescence-based melting assays for studying quadruplex ligands. *Methods* **2007**, *42*, 183–195.
(26) Rachwal, P. A.; Fox, K. R. Quadruplex melting. *Methods* **2007**, *43*, 291–301.
(27) Zhou, J.-L.; Lu, Y.-J.; Ou, T.-M.; Zhou, J.-M.; Huang, Z.-S.; Zhu, X.-F.; Du, C.-J.; Bu, X.-Z.; Ma, L.; Gu, L.-Q.; Li, Y.-M.; Chan, A. S.-C. Synthesis and evaluation of quindoline derivatives as G-quadruplex inducing and stabilizing ligands and potential inhibitors of telomerase. *J. Med. Chem.* **2005**, *48*, 7315–7321.
(28) Shirude, P. S.; Gillies, E. R.; Ladame, S.; Godde, F.; Shin-ya, K.; Huc, I.; Balasubramanian, S. Macrocyclic and helical oligoamides as a new class of G-quadruplex ligands. *J. Am. Chem. Soc.* **2007**, *129*, 11890–11891.
(29) De Cian, A.; Delemos, E.; Mergny, J.-L.; Teulade-Fichou, M.-P.; Monchaud, D. Highly efficient G-quadruplex recognition by bisquinolinium compounds. *J. Am. Chem. Soc.* **2007**, *129*, 1856–1857.
(30) Cheng, M.-K.; Modi, C.; Cookson, J. C.; Hutchinson, I.; Heald, R. A.; McCarroll, A. J.; Missailidis, S.; Tanious, F.; Wilson, W. D.; Mergny, J.-L.; Laughton, C. A.; Stevens, M. F. G. Antitumor polycyclic acridines. 20. Search for DNA quadruplex binding selectivity in a series of 8,13-dimethylquino[4,3,2-*kl*]acridinium salts: telomere-targeted agents. *J. Med. Chem.* **2008**, *51*, 963–975.
(31) Paramasivan, S.; Rujan, I.; Bolton, P. H. Circular dichroism of quadruplex DNAs: applications to structure, cation effects and ligand binding. *Methods* **2007**, *43*, 324–331.
(32) Rezler, E. M.; Seenisamy, J.; Bashyam, S.; Kim, M.-Y.; White, E.; Wilson, W. D.; Hurley, L. H. Telomestatin and diseleno sapphyrin bind selectively to two different forms of the human telomeric G-quadruplex structure. *J. Am. Chem. Soc.* **2005**, *127*, 9439–9447.

(33) Zhang, W.-J.; Ou, T.-M.; Lu, Y.-J.; Huang, Y.-Y.; Wu, W.-B.; Huang, Z.-S.; Zhou, J.-L.; Wong, K.-Y.; Gu, L.-Q. 9-Substituted berberine derivatives as G-quadruplex stabilizing ligands in telomeric DNA. *Bioorg. Med. Chem.* **2007**, *15*, 5493–5501.

(34) White, E. W.; Tanious, F.; Ismail, M. A.; Reszka, A. P.; Neidle, S.; Boykin, D. W.; Wilson, W. D. Structure-specific recognition of quadruplex DNA by organic cations: influence of shape, substituents and charge. *Biophys. Chem.* **2007**, *126*, 140–153.

(35) Ren, L.; Zhang, A.; Huang, J.; Wang, P.; Weng, X.; Zhang, L.; Liang, F.; Tan, Z.; Zhou, X. Quaternary ammonium zinc phthalocyanine: inhibiting telomerase by stabilizing G quadruplexes and inducing G-quadruplex structure transition and formation. *ChemBioChem* **2007**, *8*, 775–780.

(36) Lu, Y.-J.; Ou, T.-M.; Tan, J.-H.; Hou, J.-Q.; Shao, W.-Y.; Peng, D.; Sun, N.; Wang, X.-D.; Wu, W.-B.; Bu, X.-Z.; Huang, Z.-S.; Ma, D.-L.; Wong, K.-Y.; Gu, L.-Q. 5-*N*-Methylated quindoline derivatives as telomeric G-quadruplex stabilizing ligands: effects of 5-N positive charge on quadruplex binding affinity and cell proliferation. *J. Med. Chem.* **2008**, *51*, 6381–6392.

(37) Ambrus, A.; Chen, D.; Dai, J.; Bialis, T.; Jones, R. A.; Yang, D. Human telomeric sequence forms a hybrid-type intramolecular G-quadruplex structure with mixed parallel/antiparallel strands in potassium solution. *Nucleic Acids Res.* **2006**, *34*, 2723–2735.

(38) Luu, K. N.; Phan, A. T.; Kuryavyi, V.; Lacroix, L.; Patel, D. J. Structure of the human telomere in K^+ solution: An intramolecular (3 + 1) G-quadruplex scaffold. *J. Am. Chem. Soc.* **2006**, *128*, 9963–9970.

(39) Matsugami, A.; Xu, Y.; Noguchi, Y.; Sugiyama, H.; Katahira, M. Structure of a human telomeric DNA sequence stabilized by 8-bromoguanosine substitutions, as determined by NMR in a K^+ solution. *FEBS J.* **2007**, *274*, 3545–3556.

(40) Xue, Y.; Kan, Z.-Y.; Wang, Q.; Yao, Y.; Liu, J.; Hao, Y.-H.; Tan, Z. Human telomeric DNA forms parallel-stranded intramolecular G-quadruplex in K^+ solution under molecular crowding condition. *J. Am. Chem. Soc.* **2007**, *129*, 11185–11191.

(41) Keating, L. R.; Szalai, V. A. Parallel-stranded guanine quadruplex interactions with a copper cationic porphyrin. *Biochemistry* **2004**, *43*, 15891–15900.

(42) Parkinson, G. N.; Lee, M. P. H.; Neidle, S. Crystal structure of parallel quadruplexes from human telomeric DNA. *Nature (London)* **2002**, *417*, 876–880.

(43) Dai, J.; Punchihewa, C.; Ambrus, A.; Chen, D.; Jones, R. A.; Yang, D. Structure of the intramolecular human telomeric G-quadruplex in potassium solution: a novel adenine triple formation. *Nucleic Acids Res.* **2007**, *35*, 2440–2450.

(44) Bates, P.; Mergny, J.-L.; Yang, D. Quartets in G-major. The first international meeting on quadruplex DNA. *EMBO Rep.* **2007**, *8*, 1003–1010.

(45) Agrawal, S.; Ojha, R. P.; Maiti, S. Energetics of the human Tel-22 quadruplex−telomestatin interaction: a molecular dynamics study. *J. Phys. Chem. B* **2008**, *112*, 6828–6836.

(46) Moorhouse, A. D.; Haider, S.; Gunaratnam, M.; Munnur, D.; Neidle, S.; Moses, J. E. Targeting telomerase and telomeres: a click chemistry approach towards highly selective G-quadruplex ligands. *Mol. BioSyst.* **2008**, *4*, 629–642.

(47) Drewe, W. C.; Nanjunda, R.; Gunaratnam, M.; Beltran, M.; Parkinson, G. N.; Reszka, A. P.; Wilson, W. D.; Neidle, S. Rational design of substituted diarylureas: a scaffold for binding to G-quadruplex motifs. *J. Med. Chem.* **2008**, *51*, 7751–7767.

(48) Reed, J.; Gunaratnam, M.; Beltran, M.; Reszka Anthony, P.; Vilar, R.; Neidle, S. TRAP-LIG, a modified telomere repeat amplification protocol assay to quantitate telomerase inhibition by small molecules. *Anal. Biochem.* **2008**, *380*, 99–105.

(49) De Cian, A.; Cristofari, G.; Reichenbach, P.; De Lemos, E.; Monchaud, D.; Teulade-Fichou, M.-P.; Shin-ya, K.; Lacroix, L.; Lingner, J.; Mergny, J.-L. Reevaluation of telomerase inhibition by quadruplex ligands and their mechanisms of action. *Proc. Natl. Acad. Sci. U.S.A.* **2007**, *104*, 17347–17352.

(50) Hwang, E. S. Replicative senescence and senescence-like state induced in cancer-derived cells. *Mech. Ageing Dev.* **2002**, *123*, 1681–1694.

(51) Riou, J. F.; Guittat, L.; Mailliet, P.; Laoui, A.; Renou, E.; Petitgenet, O.; Megnin-Chanet, F.; Helene, C.; Mergny, J. L. Cell senescence and telomere shortening induced by a new series of specific G-quadruplex DNA ligands. *Proc. Natl. Acad. Sci. U.S.A.* **2002**, *99*, 2672–2677.

(52) Sumi, M.; Tauchi, T.; Sashida, G.; Nakajima, A.; Gotoh, A.; Shin-Ya, K.; Ohyashiki, J. H.; Ohyashiki, K. A. G-quadruplex-interactive agent, telomestatin (SOT-095), induces telomere shortening with apoptosis and enhances chemosensitivity in acute myeloid leukemia. *Int. J. Oncol.* **2004**, *24*, 1481–1487.

(53) Tauchi, T.; Shin-ya, K.; Sashida, G.; Sumi, M.; Okabe, S.; Ohyashiki, J. H.; Ohyashiki, K. Telomerase inhibition with a novel G-quadruplex-interactive agent, telomestatin: in vitro and in vivo studies in acute leukemia. *Oncogene* **2006**, *25*, 5719–5725.

(54) Zhou, J. M.; Zhu, X. F.; Lu, Y. J.; Deng, R.; Huang, Z. S.; Mei, Y. P.; Wang, Y.; Huang, W. L.; Liu, Z. C.; Gu, L. Q.; Zeng, Y. X. Senescence and telomere shortening induced by novel potent G-quadruplex interactive agents, quindoline derivatives, in human cancer cell lines. *Oncogene* **2006**, *25*, 503–511.

(55) Huang, F.-C.; Chang, C.-C.; Lou, P.-J.; Kuo, I. C.; Chien, C.-W.; Chen, C.-T.; Shieh, F.-Y.; Chang, T.-C.; Lin, J.-J. G-Quadruplex stabilizer 3,6-bis(1-methyl-4-vinylpyridinium)carbazole diiodide induces accelerated senescence and inhibits tumorigenic properties in cancer cells. *Mol. Cancer Res.* **2008**, *6*, 955–964.

(56) Johne, S.; Jung, B.; Groeger, D.; Radeglia, R. Synthesis and carbon-13 NMR spectroscopy of some pyrrolo[2,1-*b*]quinazolines. *J. Prakt. Chem.* **1977**, *319*, 919–26.

(57) Shakhidoyatov, K. M.; Oripov, E. O.; Yun, L. M.; Yamankulov, M. Y.; Kadyrov, C. S. Synthesis of potential fungicides in the quinazoline series. *Fungitsidy* **1980**, 66–81.

(58) Tan, J. H.; Zhang, Q. X.; Huang, Z. S.; Chen, Y.; Wang, X. D.; Gu, L. Q.; Wu, J. Y. Synthesis, DNA binding and cytotoxicity of new pyrazole emodin derivatives. *Eur. J. Med. Chem.* **2006**, *41*, 1041–1047.

(59) Frisch, M. J. ; Trucks, G. W.; Schlegel, H. B.; Scuseria, G. E.; Robb, M. A.; Cheeseman, J. R.; Montgomery, J. A., Jr.; Vreven, T.; Kudin, K. N.; Burant, J. C.; Millam, J. M.; Iyengar, S. S.; Tomasi, J.; Barone, V.; Mennucci, B.; Cossi, M.; Scalmani, G.; Rega, N.; Petersson, G. A.; Nakatsuji, H.; Hada, M.; Ehara, M.; Toyota, K.; Fukuda, R.; Hasegawa, J.; Ishida, M.; Nakajima, T.; Honda, Y.; Kitao, O.; Nakai, H.; Klene, M.; Li, X.; Knox, J. E.; Hratchian, H. P.; Cross, J. B.; Bakken, V.; Adamo, C.; Jaramillo, J.; Gomperts, R. Stratmann, R. E.; Yazyev, O.; Austin, A. J.; Cammi, R.; Pomelli, C.; Ochterski, J. W.; Ayala, P. Y.; Morokuma, K.; Voth, G. A.; Salvador, P.; Dannenberg, J. J.; Zakrzewski, V. G.; Dapprich, S.; Daniels, A. D.; Strain, M. C.; Farkas, O.; Malick, D. K.; Rabuck, A. D.; Raghavachari, K.; Foresman, J. B.; Ortiz, J. V.; Cui, Q.; Baboul, A. G.; Clifford, S.; Cioslowski, J.; Stefanov, B. B.; Liu, G.; Liashenko, A.; Piskorz, P.; Komaromi, I.; Martin, R. L.; Fox, D. J.; Keith, T.; Al-Laham, M. A.; Peng, C. Y.; Nanayakkara, A.; Challacombe, M.; Gill, P. M. W.; Johnson, B.; Chen, W.; Wong, M. W.; Gonzalez, C.; Pople, J. A. *Gaussian 03, Revision E.01*; Gaussian, Inc.: Wallingford, CT, 2004.

(60) Morris, G. M.; Goodsell, D. S.; Halliday, R. S.; Huey, R.; Hart, W. E.; Belew, R. K.; Olson, A. J. Automated docking using a Lamarckian genetic algorithm and an empirical binding free energy function. *J. Comput. Chem.* **1998**, *19*, 1639–1662.

(61) Sanner, M. F. Python: a programming language for software integration and development. *J. Mol. Graph. Model.* **1999**, *17*, 57–61.

(62) Cornell, W. D.; Cieplak, P.; Bayly, C. I.; Gould, I. R.; Merz, K. M., Jr.; Ferguson, D. M.; Spellmeyer, D. C.; Fox, T.; Caldwell, J. W.; Kollman, P. A. A second generation force field for the simulation of proteins, nucleic acids, and organic molecules. *J. Am. Chem. Soc.* **1995**, *117*, 5179–5197.

(63) Wang, J.; Wolf, R. M.; Caldwell, J. W.; Kollman, P. A.; Case, D. A. Development and testing of a general Amber force field. *J. Comput. Chem.* **2004**, *25*, 1157–1174.

(64) Hazel, P.; Huppert, J.; Balasubramanian, S.; Neidle, S. Loop-length-dependent folding of G-quadruplexes. *J. Am. Chem. Soc.* **2004**, *126*, 16405–16415.

(65) Hazel, P.; Parkinson, G. N.; Neidle, S. Predictive modelling of topology and loop variations in dimeric DNA quadruplex structures. *Nucleic Acids Res.* **2006**, *34*, 2117–2127.

(66) Darden, T.; York, D.; Pedersen, L. Particle mesh Ewald: an $N \log(N)$ method for Ewald sums in large systems. *J. Chem. Phys.* **1993**, *98*, 10089–10092.

(67) Jorgensen, W. L.; Chandrasekhar, J.; Madura, J. D.; Impey, R. W.; Klein, M. L. Comparison of simple potential functions for simulating liquid water. *J. Chem. Phys.* **1983**, *79*, 926–935.

(68) Ryckaert, J. P.; Ciccotti, G.; Berendsen, H. J. C. Numerical integration of the Cartesian equations of motion of a system with constraints: molecular dynamics of *n*-alkanes. *J. Comput. Phys.* **1977**, *23*, 327–41.

(69) Humphrey, W.; Dalke, A.; Schulten, K. VMD: visual molecular dynamics. *J. Mol. Graph.* **1996**, *14*, 33–8, plates 27−28.

(70) Kollman, P. A.; Massova, I.; Reyes, C.; Kuhn, B.; Huo, S.; Chong, L.; Lee, M.; Lee, T.; Duan, Y.; Wang, W.; Donini, O.; Cieplak, P.; Srinivasan, J.; Case, D. A.; Cheatham, T. E., III. Calculating structures and free energies of complex molecules: combining molecular mechanics and continuum models. *Acc. Chem. Res.* **2000**, *33*, 889–897.

JM801600M